Nonlinear Dyn (2018) 94:1243–1265
https://doi.org/10.1007/s11071-018-4421-9

ORIGINAL PAPER

Primary resonance analysis and vibration suppression for the harmonically excited nonlinear suspension system using a pair of symmetric viscoelastic buffers

Xiaojuan Sun · Hong Zhang · Wenjun Meng · Ronghui Zhang · Kening Li · Tao Peng

Received: 11 January 2018 / Accepted: 7 June 2018 / Published online: 25 June 2018
© Springer Nature B.V. 2018

Abstract To reduce the severity of high-magnitude vibrations and shock, end-stop buffers was used for the most suspension cabs or seats of work vehicles. This paper employs a pair of symmetric linear viscoelastic end-stops to improve the performance of a single-degree-of-freedom nonlinear suspension system under primary resonance conditions, which has cubic nonlinearity. Firstly, a piecewise symmetry tri-nonlinear model is introduced. The frequency response of relative displacement corresponding to the steady-state motion is obtained by applying the multiple-scale method, which is found to be the same with the averaging method solution. And it is further verified by numerical simulation. Its stability is then studied. Subsequently, a design criterion is proposed for jump avoidance, which is caused by the saddle-node bifurcation. Also, parametric studies are carried out to illustrate effects of design parameters for the end-stop on the isolation performance at primary resonance, including responses of the relative displacement and the absolute acceleration. The results show that with dynamic parameters properly designed by using viscoelastic end-stops, the relative displacement response can be effectively suppressed and the jump can be eliminated for both hardening and softening primary isolators. Besides, the end-stop can effectively attenuate the absolute acceleration response for a hardening primary isolator, while more damping is needed to attenuate that for a softening primary isolator, although the degree of the softening nonlinearity is mitigated. It is suggested that a moderate stiffness compared to that of the primary isolator and also a high damping of the end-stop be beneficial to both vibration isolation and jump avoidance under primary resonance conditions.

Keywords Suspension system · Symmetric viscoelastic end-stops · Piecewise nonlinearity · Primary resonance · Vibration isolation performance · Jump avoidance

X. Sun · H. Zhang · W. Meng
Shanxi Key Laboratory of Intelligent Logistics Equipments, School of Mechanical Engineering, Taiyuan University of Science and Technology, Taiyuan 030024, Shanxi, China

W. Meng
School of Mechanical Engineering, Shanxi Institute of Energy, Taiyuan 030024, Shanxi, China

R. Zhang (✉)
Guangdong Key Laboratory of Intelligent Transportation System, School of Engineering, Sun Yat-sen University, Guangzhou 510275, Guangdong, China
e-mail: zrh1981819@126.com

K. Li
State Key Laboratory of Mechanical System and Vibration, Shanghai Jiao Tong University, Shanghai 200240, China

T. Peng
College of Automobile and Transportation, Tianjin University of Technology and Education, Tianjin 300222, China

1 Introduction

For suspensions of off-road and heavy road vehicles, end-stop buffers are commonly used due to their often

exposure to low-frequency/high-amplitude vibrations and shock [1–7]. Besides, to limit the up and down motions of the chassis for safety, a leaf spring with an assistant spring could be used for suspension system [8,9]. The interactions with the buffers or the assistant springs could be induced by high-magnitude vehicle vibration under resonance conditions, which may be produced only by a small-amplitude excitation. Off-road vehicles, which often do not have a primary suspension, are known to cause high-magnitude vertical ride vibration in the vicinity of the vehicle resonant frequency supported on large and soft tires. Heavy road vehicles are mostly designed with relatively soft suspension for enhanced passenger comfort and road friendliness, which tends to be more liable to generate cab's shake when subjected to road irregularities, specifically with the drain covers and potholes [10,11]. Such resonant oscillations may cause suspension impacts against the buffers, since the suspension seat resonance or suspended cab resonance can be excited by such kinds of excitations [12].

In all aforementioned cases, the suspension with end-stop buffers turns into a vibro-impact system. The performance is strongly dependent upon the viscoelastic properties of the buffers in addition to those of the primary spring and damping components. It makes the system include multistage stiffness and damping, which results in sudden changes of damping and stiffness coefficients. Such nonlinear isolation systems recognized as piecewise smooth systems can exhibit very complex behaviors under excitations, such as bifurcation and chaos [13–17], which is important to understand for the better design and control of these systems.

Much effort has been made to study the dynamic responses and the stability of piecewise linear systems for suspension mechanisms, where the primary oscillator and the buffer or the secondary suspension both have been characterized by linear elements. That is, the stiffness and the damping are linear in a stage and change drastically to another set of linear values once a threshold is reached [17–21]. But in fact, the spring and the damping components of the suspension often have inherent nonlinear properties and will be prone to showing up at resonance [22–25]. Thus, it is indispensable to study the piecewise nonlinear systems in which the characteristics of the primary oscillator or the end-stop, or both of them, are nonlinear. Stahl and Jazar [26,27] introduced a linear secondary suspension to limit high relative displacements of the primary suspension. In order to model the inherent nonlinearities involved with real systems in high displacements, the primary suspension was assumed to have dual stiffness and damping rates. Hao et al. [28] proposed a two-sided damping constraint control strategy to improve the performance of the quasi-zero stiffness isolator. In these suspension systems, the stiffness or damping piecewise characteristics resulting from existence of clearances acted together with the nonlinearities of the primary oscillators. Although detrimental effects may be brought, it can produce beneficial effects by using the nonlinear piecewise vibration isolators with their design parameters to ensure a stable response [28–31]. One of the reasons for unstable responses is the existence of the frequency jump which is induced by the saddle-node bifurcation and may be caused both by stiffness and damping nonlinearities of the primary oscillators and by piecewise nonlinearity of the buffers. Therefore, in order to obtain the desirable vibration isolation performance, researches on jump phenomenon and jump avoidance conditions have increased in recent years. Deshpande et al. [20] and Jazar et al. [21] examined the jump avoidance conditions and their sensitivities to the design parameters for a piecewise linear vibration isolator using the average method. Also, an optimal design solution of the absolute acceleration RMS with respect to the relative displacement RMS was presented within the no-jump zones in the paper [20]. Gao and Chen [32] studied a solid and liquid mixture vibration isolator characterized by bilinear stiffness using the modified average method. The critical values of the isolator parameters were determined to avoid the frequency jump. Later, they introduced the time-delayed cubic velocity feedback control into the piecewise bilinear isolation system to improve the isolation performance [33]. A modified multiple-scale method was applied to find the frequency response, and the jump phenomenon can be suppressed through choosing appropriate feedback parameters including gain and time delay. And Cheng et al. [34] investigated the jump avoidance conditions for a quasi-zero stiffness isolator with time-delayed cubic displacement feedback.

The Duffing oscillator is representative of many nonlinear systems [23,25,35]. To suppress the nonlinear vibration of a Duffing-type suspension system at primary resonance, the present work is focused on the use of a pair of symmetric linear end-stops. The dynamic model of a single-degree-of-freedom (single-d. f.) nonlinear system examined is presented in the following

section, together with a set of motion normalized equations. The relative displacement response of the system is obtained by applying the method of multiple scales, which has been used by Gao and Chen [33] and Cheng et al. [34] to calculate the frequency responses of the bilinear stiffness isolator and the quasi-zero stiffness isolator both controlled by time-delayed cubic displacement feedback. The result is compared with that obtained by the averaging method [8,18–21,26–28], which has been commonly employed because it can provide a closed form of frequency response function which is useful for parameter design in engineering practice but involves relatively less computation process. Also numerical results are presented to verify the analytical predictions. In Sect. 3, a procedure for determining the response stability characteristics is presented. In Sect. 4, effect of the end-stops is illustrated on the relative displacement response of the piecewise system, compared with that on the system without end-stops. And three cases are considered: when $\rho = 0$ in Sect. 4.1, when $\xi_2 = 0$ in Sect. 4.2 and when ρ, ξ_2 and d are all positive in Sect. 4.3. In Sect. 5, conditions of jump avoidance are investigated which should take into account both the jump-up frequency of the duffing-type primary oscillator and the state when the mass touches the end-stop. Then, the first-order approximation of the absolute acceleration response is given in Sect. 6. Effect of the end-stops on the absolute acceleration response is also analyzed. Finally, the study concludes by summarizing the most important analytical and numerical findings in Sect. 7.

2 Mechanical model and perturbation analysis

An elementary single-d. f. vibration isolator model with a pair of symmetric elastomeric end-stops is considered as shown in Fig. 1, which can be used to describe a cab or seat suspension system using end-stop buffers when the suspension is adequately adjusted to the mid-position. As attention is focused on the examination of the primary resonance, it is necessary to consider nonlinear characteristics of the primary suspension. Here, mass m is suspended on a primary isolator having linear viscous damping and Duffing-type stiffness. End-stops come into action mainly in domain around resonance which is only during a short period of time. So a linear assumption for

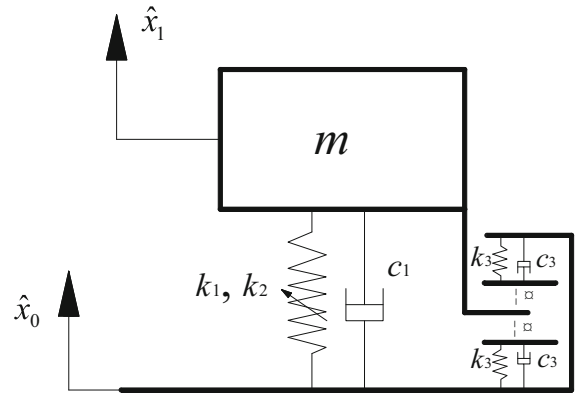


Fig. 1 An elementary single-d. f. model of a suspension system with a pair of symmetric elastomeric end-stops

the elastomeric end-stops is reasonable. Accordingly, the equation of motion of the system can be written as

$$m\frac{\mathrm{d}^2\hat{x}_1}{\mathrm{d}t^2} + k_1\hat{y} + k_2\hat{y}^3 + c_1\frac{\mathrm{d}\hat{y}}{\mathrm{d}t} + g\left(\hat{y}, \frac{\mathrm{d}\hat{y}}{\mathrm{d}t}\right) = 0 \quad (1)$$

with $\hat{y} = \hat{x}_1 - \hat{x}_0$, where $k_1 > 0$, k_1 and k_2 are, respectively, the linear and nonlinear stiffness coefficients, c_1 is the linear damping coefficient, $\hat{x}_1$ is the absolute displacement response and $\hat{x}_0$ is the base displacement excitation. If $k_2 > 0$, the primary isolator is hardening, and if $k_2 < 0$, the primary isolator is softening. The force developed in the pair of symmetric end-stops is given by

$$g\left(\hat{y}, \frac{\mathrm{d}\hat{y}}{\mathrm{d}t}\right) = \begin{cases} k_3(\hat{y} - \Delta) + c_3\frac{\mathrm{d}\hat{y}}{\mathrm{d}t} & \hat{y} > \Delta \\ 0 & -\Delta \le \hat{y} \le \Delta \\ k_3(\hat{y} + \Delta) + c_3\frac{\mathrm{d}\hat{y}}{\mathrm{d}t} & \hat{y} < -\Delta \end{cases}$$

where k_3 and c_3 are the stiffness and damping coefficients of the end-stops, and Δ ($\Delta > 0$) is the symmetric free travel of the primary isolator.

It is assumed that the system is subjected to a motion excitation as $\hat{x}_0 = u_0\cos(\Omega t)$. Using the following dimensionless system parameters:

$$\tau = \omega_1 t, \quad \omega_1^2 = \frac{k_1}{m}, \quad y = \frac{\hat{y}}{u_0}, \quad \mu = \frac{k_2 u_0^2}{k_1},$$
$$2\xi_1 = \frac{c_1}{m\omega_1}, \quad \omega_2^2 = \frac{k_3}{m}, \quad 2\xi_2 = \frac{c_3}{m\omega_1}, \quad \lambda = \frac{\Omega}{\omega_1},$$
$$d = \frac{\Delta}{u_0}, \quad \rho = \frac{\omega_2}{\omega_1},$$

Equation (1) can be written in non-dimensional form as

$$\ddot{y} + y + \mu y^3 + 2\xi_1\dot{y} + G(y, \dot{y}) = \lambda^2\cos\lambda\tau \quad (2)$$

with

$$G(y,\dot{y}) = [\rho^2(y-d)+2\xi_2\dot{y}]H(y-d) + [\rho^2(y+d)+2\xi_2\dot{y}]H(-y-d) = \begin{cases} \rho^2(y-d)+2\xi_2\dot{y} & y>d \\ 0 & -d\le y\le d \\ \rho^2(y+d)+2\xi_2\dot{y} & y<-d \end{cases}$$

where dot denotes differentiation with respect to the transformed time τ and $H(\cdot)$ is the Heaviside step function defined as

$$H(y-d) = \begin{cases} 1 & y>d \\ 0 & y\le d \end{cases},$$

$$H(-y-d) = \begin{cases} 1 & y<-d \\ 0 & y\ge -d \end{cases}.$$

Letting $f=\lambda^2$, perturbation analysis requires Eq. (2) to be rescaled as

$$\ddot{y}+y+\varepsilon\mu_1 y^3+2\varepsilon\xi_{11}\dot{y}+\varepsilon\left[\rho_1^2(y-d)+2\xi_{21}\dot{y}\right] H(y-d)+\varepsilon\left[\rho_1^2(y+d)+2\xi_{21}\dot{y}\right]H(-y-d) = \varepsilon f_1\cos\lambda\tau \tag{3}$$

where ε is a non-dimensional small parameter. All damping terms and nonlinear terms in Eq. (2) are assumed to be small and have been rescaled in terms of $\mu=\varepsilon\mu_1, \xi_1=\varepsilon\xi_{11}, \xi_2=\varepsilon\xi_{21}$ and $\rho=\sqrt{\varepsilon}\rho_1$. The amplitude of the excitation has been rescaled in terms of $f=\varepsilon f_1$ to account for the primary resonance.

To analyze the primary resonance on the natural frequency ω_1, the detuning parameter σ is introduced by the following equality:

$$\lambda^2 = 1+\varepsilon\sigma \tag{4}$$

Thus, Eq. (3) can be rewritten as

$$\ddot{y}+\lambda^2 y-\varepsilon\sigma y+\varepsilon\mu_1 y^3+2\varepsilon\xi_{11}\dot{y} +\varepsilon\left[\rho_1^2(y-d)+2\xi_{21}\dot{y}\right]H(y-d) +\varepsilon\left[\rho_1^2(y+d)+2\xi_{21}\dot{y}\right]H(-y-d) = \varepsilon f_1\cos\lambda\tau \tag{5}$$

Then, the multiple scales method is used with the following approximate solution [36–39]:

$$y(\tau;\varepsilon) = y_0(T_0,T_1)+\varepsilon y_1(T_0,T_1)+O(\varepsilon^2) \tag{6}$$

where $T_0=\tau$ is the so-called fast timescale, and $T_1=\varepsilon\tau$ is a slow timescale.

The Heaviside function $H(\cdot)$ can be expanded as

$$H(y-d) = H(y_0-d)+\varepsilon\delta(y_0-d)y_1 \tag{7}$$

$$H(-y-d) = H(-y_0-d)-\varepsilon\delta(-y_0-d)y_1 \tag{8}$$

where $\delta(\cdot)$ is the Dirac delta function.

Substituting Eq. (6) into Eq. (5), using Eqs. (7) and (8), and then collecting the terms with the identical powers of ε, we have

$$\varepsilon^0: \quad D_0^2 y_0+\lambda^2 y_0 = 0 \tag{9}$$

$$\varepsilon^1: \quad D_0^2 y_1+\lambda^2 y_1 = -2D_0D_1y_0+\sigma y_0-\mu_1 y_0^3-2\xi_{11}D_0y_0 -\left[\rho_1^2(y_0-d)+2\xi_{21}D_0y_0\right]H(y_0-d) -\left[\rho_1^2(y_0+d)+2\xi_{21}D_0y_0\right]H(-y_0-d)+f_1\cos\lambda T_0 \tag{10}$$

The general solution of Eq. (9) can be expressed as

$$y_0 = A(T_1)\cos(\lambda T_0+\phi(T_1)) \tag{11}$$

where A is the response amplitude, $A>0$, and ϕ is the phase, both of which are functions of T_1. Considering $\gamma=\lambda T_0+\phi$ and substituting Eq. (11) into Eq. (10), we obtain

$$D_0^2 y_1+\lambda^2 y_1 = 2\lambda A'\sin\gamma+2\lambda A\phi'\cos\gamma +\sigma A\cos\gamma-\mu_1 A^3\cos^3\gamma +2\xi_{11}\lambda A\sin\gamma -\left[\rho_1^2(A\cos\gamma-d)-2\xi_{21}\lambda A\sin\gamma\right]H(A\cos\gamma-d) -\left[\rho_1^2(A\cos\gamma+d)-2\xi_{21}\lambda A\sin\gamma\right]H(-A\cos\gamma-d) +f_1\cos(\gamma-\phi) \tag{12}$$

As $H(A\cos\gamma-d)$ and $H(-A\cos\gamma-d)$ are periodic function with circular frequency of λ, they can be expanded as the following Fourier series:

$$H(A\cos\gamma-d) = \frac{a_0}{2}+\sum_{n=1}^{\infty}a_n\cos n\gamma \tag{13}$$

$$H(-A\cos\gamma-d) = \frac{a_0}{2}+\sum_{n=1}^{\infty}(-1)^n a_n\cos n\gamma \tag{14}$$

where $a_n = \frac{2\sin n\theta}{n\pi}$, $(n=0,\ 1,\ 2)$ and $\theta = \begin{cases} \arccos\frac{d}{A}\in(0,\ \frac{\pi}{2}) & A>d \\ 0 & A\le d \end{cases}$.

Then, substitution of Eqs. (13) and (14) into Eq. (12) gives

$$
\begin{aligned}
&D_0^2 y_1 + \lambda^2 y_1 \\
&\quad = 2\lambda A' \sin\gamma + 2\lambda A\phi' \cos\gamma + \sigma A \cos\gamma \\
&\qquad - \mu_1 A^3 \cos^3\gamma + 2\xi_{11}\lambda A \sin\gamma \\
&\qquad - [\rho_1^2 (A\cos\gamma - d) - 2\xi_{21}\lambda A \sin\gamma] \\
&\qquad \left[\frac{a_0}{2} + \sum_{n=1}^{\infty} a_n \cos n\gamma\right] \\
&\qquad - [\rho_1^2 (A\cos\gamma + d) - 2\xi_{21}\lambda A \sin\gamma] \\
&\qquad \left[\frac{a_0}{2} + \sum_{n=1}^{\infty} (-1)^n a_n \cos n\gamma\right] + f_1 \cos(\gamma - \phi) \\
&\quad = 2\lambda A' \sin\gamma + 2\lambda A\phi' \cos\gamma + \sigma A \cos\gamma \\
&\qquad - \frac{1}{4}\mu_1 A^3 \left[3\cos\gamma + \cos 3\gamma\right] + 2\xi_{11}\lambda A \sin\gamma \\
&\qquad - \left\{\rho_1^2 a_0 A \cos\gamma + 2\rho_1^2 A \cos\gamma \sum_{n=1}^{\infty} a_{2n} \cos 2n\gamma \right. \\
&\qquad\quad - 2d\rho_1^2 \sum_{n=0}^{\infty} a_{2n+1} \cos(2n+1)\gamma \\
&\qquad\quad - 2\xi_{21} a_0 \lambda A \sin\gamma \\
&\qquad\quad \left. - 4\xi_{21}\lambda A \sin\gamma \sum_{n=1}^{\infty} a_{2n} \cos 2n\gamma \right\} \\
&\qquad\quad + f_1 \cos(\gamma - \phi) \\
&\quad = f_1 \cos(\gamma - \phi) + \left(2\lambda A\phi' + \sigma A - \frac{3}{4}\mu_1 A^3\right) \\
&\qquad \cos\gamma + (2\lambda A' + 2\xi_{11}\lambda A) \sin\gamma - \frac{1}{4}\mu_1 A^3 \cos 3\gamma \\
&\qquad + \sum_{n=0}^{\infty} (2d\rho_1^2 a_{2n+1} - \rho_1^2 A a_{2n} - \rho_1^2 A a_{2n+2}) \\
&\qquad \cos(2n+1)\gamma \\
&\qquad + 2\xi_{21}\lambda A \sum_{n=0}^{\infty} (a_{2n} - a_{2n+2}) \sin(2n+1)\gamma \qquad (15)
\end{aligned}
$$

Eliminating the secular terms from y_1, we obtain from Eq. (15) that

$$
\begin{aligned}
&f_1 \sin\phi + (2\lambda A' + 2\xi_{11}\lambda A) \\
&\quad + 2(a_0 - a_2)\xi_{21}\lambda A = 0 \qquad (16) \\
&f_1 \cos\phi + \left(2\lambda A\phi' + \sigma A - \frac{3}{4}\mu_1 A^3\right) \\
&\quad + 2d\rho_1^2 a_1 - \rho_1^2 A(a_0 + a_2) = 0 \qquad (17)
\end{aligned}
$$

They can be rewritten as

$$
2\lambda A' = -2\xi_{11}\lambda A - 2(a_0 - a_2)\xi_{21}\lambda A - f_1 \sin\phi \qquad (18)
$$

$$
\begin{aligned}
2\lambda A\phi' = &-\frac{\lambda^2 - 1}{\varepsilon} A + \frac{3}{4}\mu_1 A^3 - 2d\rho_1^2 a_1 \\
&+ \rho_1^2 (a_0 + a_2) A - f_1 \cos\phi \qquad (19)
\end{aligned}
$$

Considering the steady-state response where $A' = 0$ and $\phi' = 0$, we obtain from Eqs. (18) and (19)

$$
2\xi_{11}\lambda A + 2(a_0 - a_2)\xi_{21}\lambda A + f_1 \sin\phi = 0 \qquad (20)
$$

$$
\begin{aligned}
&\left[\rho_1^2 (a_0 + a_2) - \frac{\lambda^2 - 1}{\varepsilon}\right] A + \frac{3}{4}\mu_1 A^3 \\
&\quad - 2d\rho_1^2 a_1 - f_1 \cos\phi = 0 \qquad (21)
\end{aligned}
$$

Then, using the identity $\sin^2\phi + \cos^2\phi = 1$ yields

$$
\begin{aligned}
&\left\{\left[\rho_1^2 (a_0 + a_2) - \frac{\lambda^2 - 1}{\varepsilon}\right] A + \frac{3}{4}\mu_1 A^3 - 2d\rho_1^2 a_1\right\}^2 \\
&\quad + [2\xi_{11} + 2(a_0 - a_2)\xi_{21}]^2 \lambda^2 A^2 = f_1^2 \qquad (22)
\end{aligned}
$$

Multiplying both sides by ε^2, the frequency-response relation is obtained as

$$
\begin{aligned}
&\left\{[\rho^2 (a_0 + a_2) - (\lambda^2 - 1)] A + \frac{3}{4}\mu A^3 - 2d\rho^2 a_1\right\}^2 \\
&\quad + [2\xi_1 + 2(a_0 - a_2)\xi_2]^2 \lambda^2 A^2 = \lambda^4 \qquad (23)
\end{aligned}
$$

which is an implicit function of the amplitude A and the frequency λ. Also, it can be found that it is irrelevant to the value of the small parameter ε. Compared with the solution derived by applying the averaging method according to the Refs. [26,27] as shown in "Appendix A," it can be seen that the two results are in agreement with each other.

Defining

$$
R_1(A) = \rho^2 (a_0 + a_2) - 2\frac{d}{A}\rho^2 a_1 = \rho^2 (a_0 - a_2) \qquad (24)
$$

and

$$
R_2(A) = 2\xi_2 (a_0 - a_2), \qquad (25)
$$

the frequency-response equation of the piecewise system can be rearranged as

$$
\begin{aligned}
&A^2 \left(\lambda^2 - \left(1 + \frac{3}{4}\mu A^2\right) - R_1\right)^2 \\
&\quad + A^2 (2\xi_1 + R_2)^2 \lambda^2 = \lambda^4 \qquad (26)
\end{aligned}
$$

The backbone curve is then given by

$$\lambda^2 = 1 + \frac{3}{4}\mu A^2 + R_1 \tag{27}$$

Equation (26) can also be expanded and arranged as

$$(A^2 - 1)\lambda^4 + B_1\lambda^2 + B_0 = 0 \tag{28}$$

where $B_1 = (2\xi_1 + R_2)^2 A^2 - 2A^2\left(1 + \frac{3}{4}\mu A^2 + R_1\right)$ and $B_0 = A^2\left(1 + \frac{3}{4}\mu A^2 + R_1\right)^2$

When $A \neq 1$, Eq. (28) is quadratic in λ^2. The discriminant D is given by

$$D = B_1^2 - 4B_0(A^2 - 1) \tag{29}$$

Solving for λ in Eq. (28), the two positive solutions are

$$\lambda_{1,2} = \left(\frac{-B_1 \pm (D)^{1/2}}{2(A^2 - 1)}\right)^{1/2} \tag{30a,b}$$

These equations yield real values of λ provided that

$$D \geq 0 \tag{31}$$

and also

$$\frac{-B_1 \pm (D)^{1/2}}{2(A^2 - 1)} \geq 0 \tag{32a,b}$$

When $A = 1$, Eq. (28) is quadratic in λ and the positive solution is

$$\lambda = \left(-\frac{B_0}{B_1}\right)^{1/2} \tag{33}$$

Since $B_0 > 0$, this equation yields real value of λ provided that

$$B_1 < 0 \tag{34}$$

It is a point belonging to the left part of the frequency response curve since the right part for the relative displacement transmissibility should be close to unity.

The two cases of $A \neq 1$ and $A = 1$ can be combined to give the solutions of Eq. (28) as

$$\lambda_1 = \left(\frac{-B_1 + (D)^{1/2}}{2(A^2 - 1)}\right)^{1/2} \tag{35a}$$

which should satisfy the inequalities of Eqs. (31) and (32a), and

$$\lambda_2 = \begin{cases} \left(\frac{-B_1 - (D)^{1/2}}{2(A^2-1)}\right)^{1/2} & A \neq 1 \\ \left(-\frac{B_0}{B_1}\right)^{1/2} & A = 1 \end{cases} \tag{35b}$$

which should satisfy the inequalities of Eqs. (31) and (32b) when $A \neq 1$ and satisfy Eq. (34) when $A = 1$.

As shown in Fig. 2, the frequency response curves of the piecewise system are plotted, calculated using Eq. (35a) and (35b) for the range of A that satisfies the inequalities of Eqs. (31), (32a,b) and (34). The backbone curves are plotted using Eq. (27). Also, the perturbation method results are compared with the numerical results obtained through the classical fourth-order Runge–Kutta algorithm according to Eq. (2). It can be seen that the approximate solutions and the numerical solutions are in an excellent agreement for the case of primary resonance. Those solution branches represented by the broken lines are unstable, which cannot be estimated by the numerical simulation. They will be analyzed detailedly in the following section.

3 Stability analysis

According to Eqs. (18) and (19) and using Eqs. (24) and (25), we have

$$2\lambda A' = -2\xi_{11}\lambda A - \frac{R_2\lambda A}{\varepsilon} - f_1 \sin\phi \tag{36}$$

$$2\lambda A\phi' = -\frac{\lambda^2 - 1}{\varepsilon}A + \frac{3}{4}\mu_1 A^3 + \frac{R_1 A}{\varepsilon} - f_1\cos\phi \tag{37}$$

For the steady-state response,

$$f_1 \sin\phi = -2\xi_{11}\lambda A - \frac{R_2\lambda A}{\varepsilon} \tag{38}$$

$$f_1\cos\phi = -\frac{\lambda^2 - 1}{\varepsilon}A + \frac{3}{4}\mu_1 A^3 + \frac{R_1 A}{\varepsilon} \tag{39}$$

To implement the stability of the stationary solutions at (A_0, ϕ_0) from Eqs. (36) and (37), a small variation $\mathbf{v} = [\alpha, \beta]^{\mathrm{T}}$ near the steady state is introduced as

$$A = A_0 + \alpha, \quad \phi = \phi_0 + \beta \tag{40a,b}$$

Substituting Eqs. (40a) and (40b) into Eqs. (36) and (37) and expanding the equations in a Taylor series yield

$$\alpha' = -\xi_{11}\alpha - \frac{R_2'(A_0)A_0 + R_2(A_0)}{2\varepsilon}\cdot\alpha - \frac{f_1}{2\lambda}\cos\phi_0 \cdot \beta \tag{41}$$

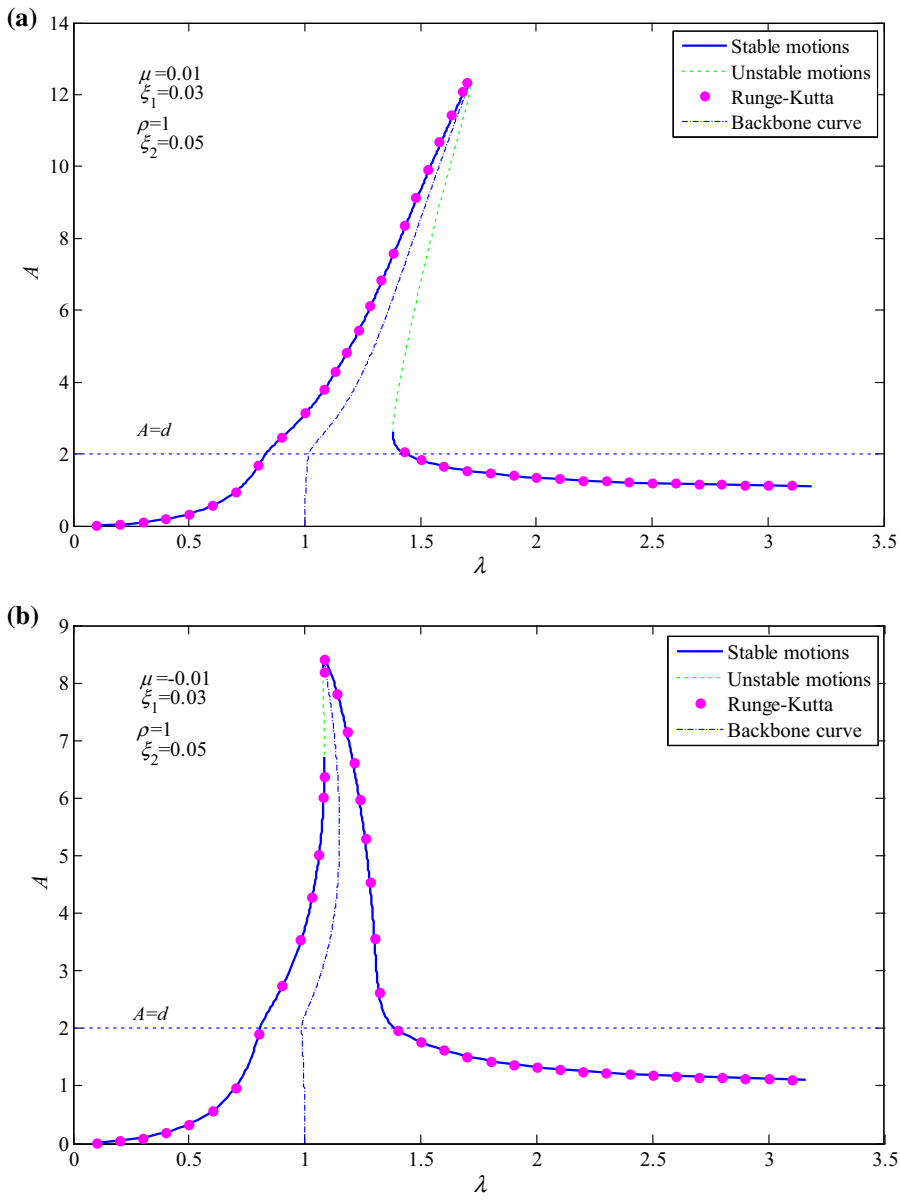


Fig. 2 Comparison between analytical and numerical frequency responses

$$\beta' = \left(\frac{3}{4\lambda}\mu_1 A_0 + \frac{R_1'(A_0)}{2\varepsilon\lambda} + \frac{f_1}{2\lambda A_0^2}\cos\phi_0\right)\alpha + \left(\frac{f_1}{2\lambda A_0}\sin\phi_0\right)\beta \tag{42}$$

where R_1' and R_2' are, respectively, the derivatives of R_1 and R_2 with respect to A, given in "Appendix B."

Equations (41) and (42) are written in state-space form by using Eqs. (38) and (39) as

$$\mathbf{v}' = \mathbf{B}\mathbf{v} = \begin{pmatrix} b_{11} & b_{12} \\ b_{21} & b_{22} \end{pmatrix}\mathbf{v} \tag{43}$$

where

$$b_{11} = -\xi_{11} - \frac{R_2'(A_0)A_0 + R_2(A_0)}{2\varepsilon},$$

$$b_{12} = -\frac{1}{2\lambda}\left(-\frac{\lambda^2-1}{\varepsilon}A_0 + \frac{3}{4}\mu_1 A_0^3 + \frac{R_1(A_0)A_0}{\varepsilon}\right),$$

$$b_{21} = \frac{9}{8\lambda}\mu_1 A_0 + \frac{R_1'(A_0)}{2\varepsilon\lambda} + \frac{R_1(A_0)}{2\varepsilon\lambda A_0} - \frac{\lambda^2-1}{2\varepsilon\lambda A_0},$$

$$b_{22} = -\xi_{11} - \frac{R_2(A_0)}{2\varepsilon}.$$

The stability at the steady state (A_0, ϕ_0) depends on the eigenvalues of the coefficient matrix **B**. Only when the following conditions are satisfied simultaneously:

$$b_{11} + b_{22} < 0 \tag{44}$$

$$b_{11}b_{22} - b_{12}b_{21} > 0, \tag{45}$$

the steady-state motions are asymptotically stable [36]. In practice, the damper and the end-stop of the suspension always have positive damping. And the natural frequency of the system and the excitation frequency are always positive. Therefore, condition (44) could always be satisfied. Thus, the equation $b_{11}b_{22} - b_{12}b_{21} = 0$ defines the stability boundary and indicates the occurrence of a saddle-node bifurcation, which means that the jump phenomenon will occur.

4 Effects of end-stop parameters on resonance responses

In this section, keeping μ and ξ_1 constant, primary resonance response curves are obtained for parameters ρ, ξ_2 and d of the end-stop varying. In all these diagrams, the solid lines represent stable motions, while the dashed lines represent unstable motions. The dash-dotted lines represent backbone curves. And the dotted lines represent conditions of $A = d$. The jump phenomenon occurs at critical points of the stable and unstable regions when the frequency is increasing or decreasing. Firstly, the cases of $\rho = 0$ and $\xi_2 = 0$ are investigated in order to study effects of parameters ξ_2 and ρ on primary resonance performance of the studied system, respectively. Then, the case of parameters ρ, ξ_2 and d all positive is investigated to further examine effects of parameters ρ and d.

4.1 Case I: $\rho = 0$

As seen from Eqs. (24) and (27), the parameter ξ_2 is irrelevant to the backbone curve. As shown in Fig. 3, the degree of nonlinearity is not changed when ξ_2 varies. On the other hand, increase of the damping ratio, ξ_2, results in amplitude reduction of frequency responses and in decrease of unstable motion zones for fixed value of d. Therefore, using a pair of symmetric damping end-stops has benefit to the primary resonance attenuation for a nonlinear oscillator, which is also consistent with the result obtained by Stahl and Jazar [26,27] and Hao et al. [28].

4.2 Case II: $\xi_2 = 0$

Letting $\xi_2 = 0$, R_2 will be zero and frequency-response Eq. (26) will become as $A^2\left(\lambda^2 - \left(1 + \frac{3}{4}\mu A^2\right) - R_1\right)^2 + 4\xi_1^2 A^2\lambda^2 = \lambda^4$. As shown in Fig. 3, compared with the system with no stops, the backbone curves shift toward the right when $A > d$. In Fig. 3a, there is no jump-down frequencies for the hardening systems both with no end-stops (a duffing-type isolator system) and with end-stops when $\mu = 0.01$ and $\xi_1 = 0.03$. In Fig. 3b, the peak amplitudes increase for the duffing-type systems with end-stops. It can be seen that the primary resonance isolation performance becomes worse when using a pair of symmetric positive stiffness constraints.

4.3 Case III: ρ, ξ_2 and d are all positive

The benefit of increase of the end-stop damping is obvious as shown in Fig. 3, and it is also obtained in Refs. [26–28]. In this subsection, the values of the design parameters for the end-stop, ρ and d, are varied independently and their effects on the frequency response are examined further as shown in Figs. 4 and 5, respectively. Compared with the duffing-type system with no stops, under primary resonance conditions, these illustrative examples show the effectiveness of the linear viscoelastic end-stop for suppressing the nonlinear vibration of the duffing-type suspension system.

As observed in Fig. 4, the value of ρ varies from 0 to 2 for fixed values of ξ_2 and d. A higher magnitude of ρ results in a higher peak amplitude and a backbone curve bending more severely to the right. That is, positive stiffness of the end-stop brings a hard nonlinearity to the system. Consequently, as shown in Fig. 4a for a hardening primary isolator, compared with damping constraints ($\rho = 0$), it will deteriorate the isolation performance on primary resonance by using a pair of symmetric viscoelastic end-stops. But on the other hand, as shown in Fig. 4b, unstable motion zones decrease when $\rho = 0.5$ and $\rho = 1$ for a softening primary isolator. Therefore, a too stiff end-stop, stiff when compared

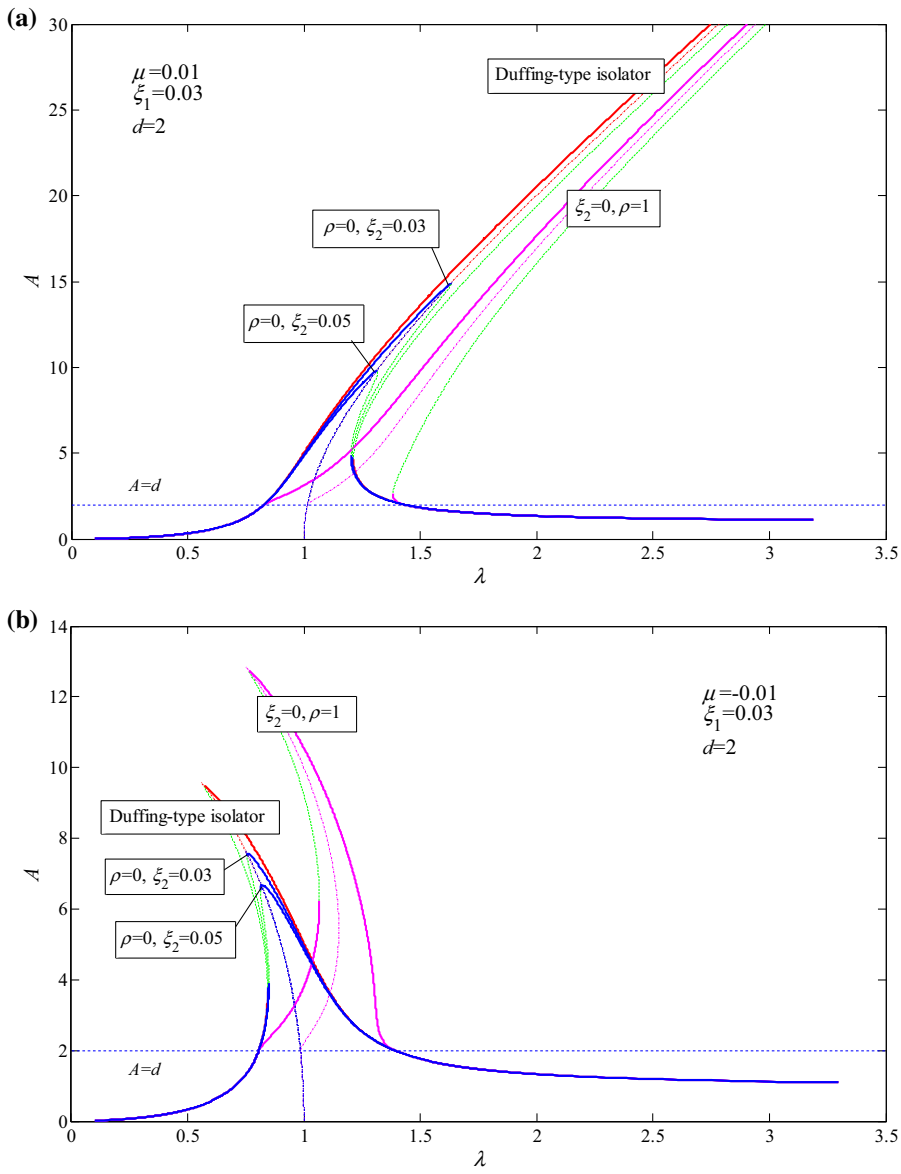


Fig. 3 Frequency-response curves of nonlinear piecewise systems when $\rho = 0$ or when $\xi_2 = 0$ compared with corresponding duffing-type oscillators

with the primary isolator, can be detrimental to the primary resonance reduction, which is consistent with the result obtained by Stahl and Jazar [26].

Figure 5 presents a series of response diagrams to evaluate the variation effect of the free travel d on the frequency response for fixed values of ρ and ξ_2. It can be seen that a smaller free travel makes the backbone curve bend to more right, which means a smaller free travel makes the system more hardening. Moreover, end-stop impacts should be avoided in the case of low-amplitude vibrations or in the absence of intense impulsive excitations. Therefore, it necessitates a minimal free travel [40–42]. In addition, a smaller d decreases the amplitude of the frequency response as shown in Fig. 5a, b, while it increases the amplitude of the frequency response for a stronger softening primary system as shown in Fig. 5c, which is one case studied by Stahl and Jazar [26]. But compared with the response curves in Fig. 5d, it can be seen that if there is enough damping of the end-stop in the stronger softening primary system, the response amplitude will decrease for a smaller free travel.

Therefore, the design parameters, ρ, ξ_2 and d, have interactive influence of each other on the primary reso-

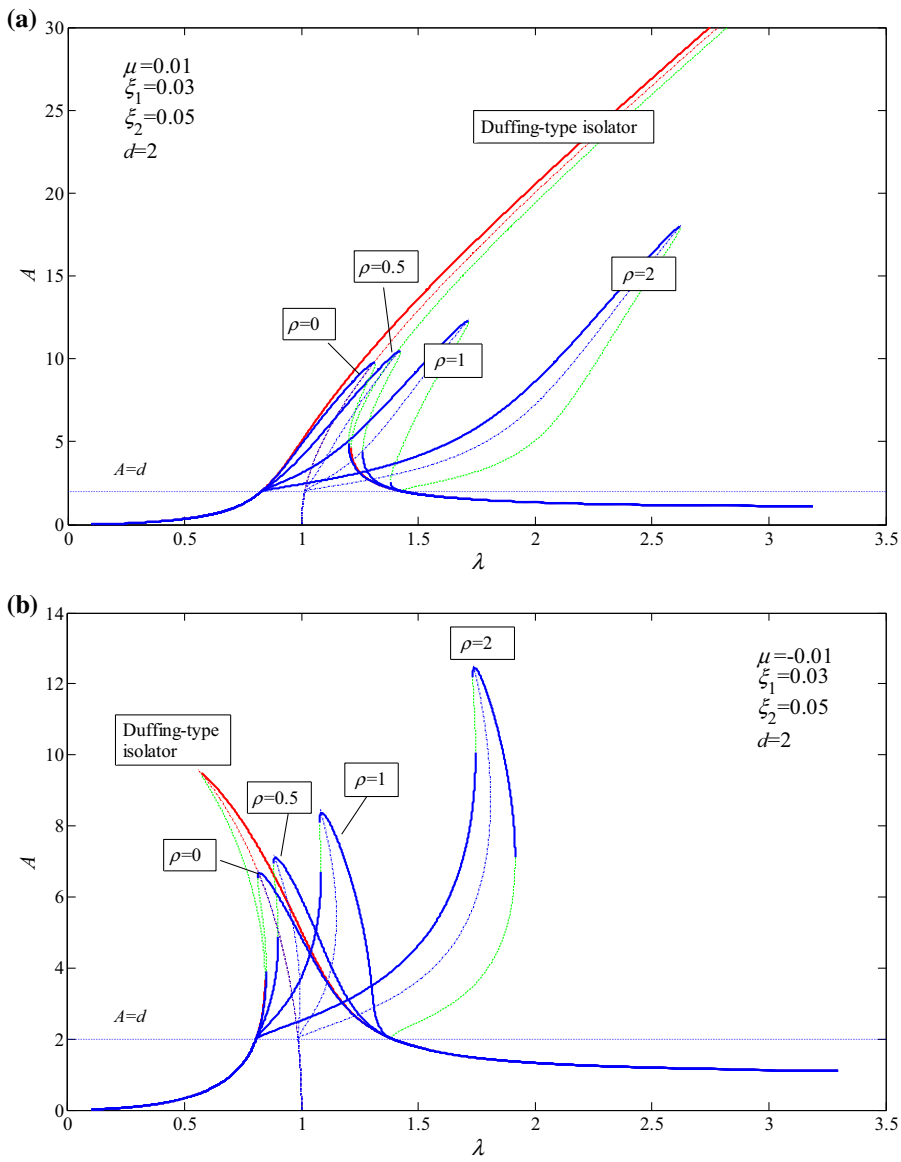


Fig. 4 Frequency-response curves for various values of stiffness ratio ρ

nance performance of the system examined. And also, the parameter effects are dependent on the degree of nonlinearity and the damping of primary isolator.

5 Conditions for jump avoidance

Through above analysis, jump will not occur within a particular range of the parameters ρ, ξ_2 and d as well as μ and ξ_1. In fact, the jump can be avoided if it can be ensured that the frequency response of the system is unique [20,21]. It is known the duffing-type isolator brings a softening or a hardening nonlinearity dependent on the sign of μ. And the linear end-stop brings a hardening nonlinearity because of the linear stiffness ρ and the free travel d. Therefore, to investigate jump avoidance conditions, we should examine the cases of $A \leq d$ and $A > d$ separately. When $A \leq d$, only the primary isolator works. The jump frequencies and the corresponding displacement amplitudes for the duffing oscillator have been determined by Brennan et al. [43], who also studied the effect of nonlinearity and damping on the occurrence of the jump phenomena. There is a threshold value of μ where the jump will occur. Thus, when the jump exists in the duffing-type primary

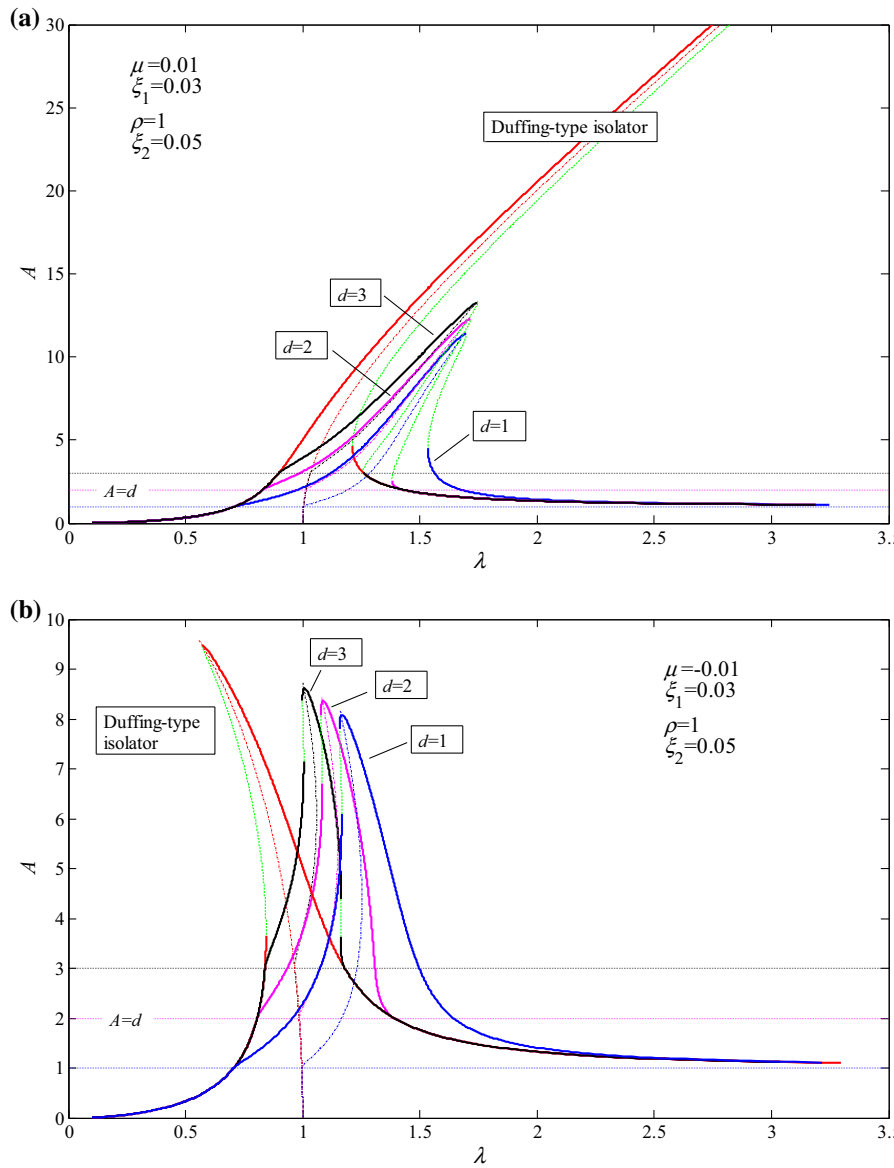


Fig. 5 Frequency-response curves for various values of free travel d

system, jump avoidance can be ensured in the range of $A \leq d$ if the free travel d can be less than the amplitude A_u at the jump-up frequency λ_u which is strongly dependent upon the nonlinear parameter μ. Next, if the frequency response curve is single-valued when $A > d$, jump avoidance can be ensured in the present piecewise suspension system [44–47].

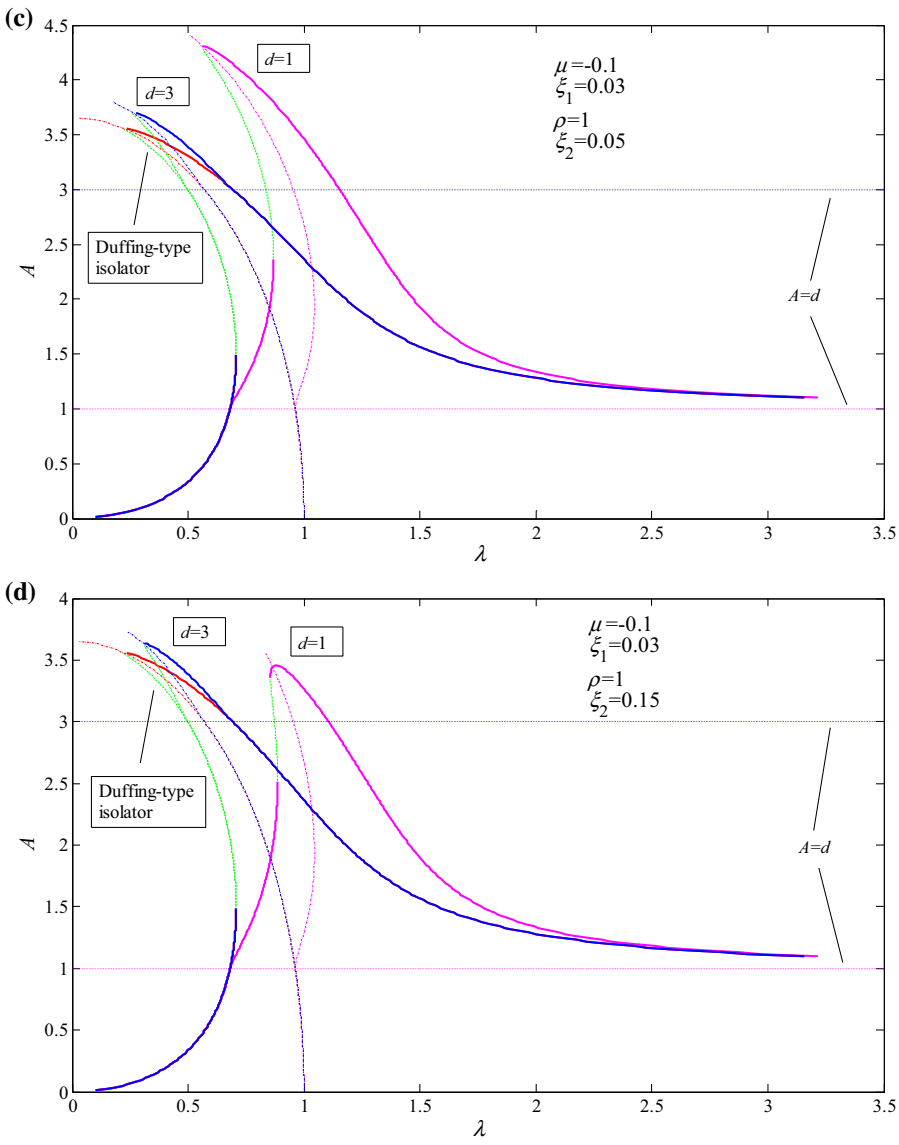
When there are no end-stops, frequency-response equation of the primary isolator system can be written as

$$A^2\left(\lambda^2-\left(1+\frac{3}{4}\mu A^2\right)\right)^2+4A^2\xi_1^2\lambda^2=\lambda^4 \tag{46}$$

based on Eq. (26). The relative displacement amplitude of the primary isolator at the jump-up frequency can be determined by using Eq. (46) and solving $\frac{\mathrm{d}\lambda}{\mathrm{d}A}=0$ for A according to the paper [43]. Differentiating both sides of Eq. (46) with respect to the amplitude A yields

$$\begin{aligned}&2\left(-(\lambda^2-1)A+\frac{3}{4}\mu A^3\right)\\&\left(-(\lambda^2-1)-2A\lambda\frac{\mathrm{d}\lambda}{\mathrm{d}A}+\frac{9}{4}\mu A^2\right)\\&+4\xi_1\lambda A\left(2\xi_1\lambda+2\xi_1 A\frac{\mathrm{d}\lambda}{\mathrm{d}A}\right)=4\lambda^3\frac{\mathrm{d}\lambda}{\mathrm{d}A}\end{aligned} \tag{47}$$

Fig. 5 continued



Substituting $\frac{\mathrm{d}\lambda}{\mathrm{d}A} = 0$ into Eq. (47) yields

$$\left(-(\lambda^2-1)A+\frac{3}{4}\mu A^3\right)\left(-(\lambda^2-1)+\frac{9}{4}\mu A^2\right)+4\xi_1^2\lambda^2 A=0 \tag{48}$$

This can be expanded and arranged as

$$\frac{27}{16}\mu^2A^4+3\mu(1-\lambda^2)A^2+\lambda^4+(4\xi_1^2-2)\lambda^2+1=0 \tag{49}$$

Solving for A in Eq. (49) gives

$$A_{1,2}=\frac{2}{3}\left(\frac{2(\lambda^2-1)\pm\left(\lambda^4-12\xi_1^2\lambda^2-2\lambda^2+1\right)^{1/2}}{\mu}\right)^{1/2} \tag{50a,b}$$

which can be combined with Eqs. (31), (32a,b) and (34) in the condition of $R_1 = R_2 = 0$ to give the jump-up frequency λ_u and its corresponding amplitude A_u, as shown in Fig. 6. In Eqs. (50a,b) the + sign is corresponding to the jump-up frequency for the softening system when $\mu < 0$, and the – sign is corresponding to

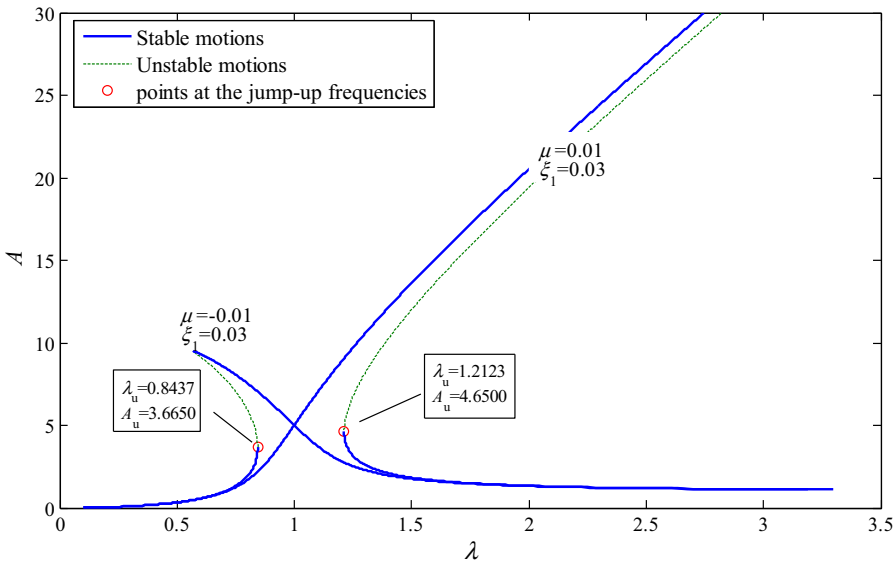


Fig. 6 Jump-up frequencies and their corresponding amplitudes for Duffing-type primary isolators

the jump-up frequency for the hardening system when $\mu > 0$.

For the jump not to occur in the range of $A \leq d$, the following condition is necessary:

$$d < A_u \tag{51}$$

When $A > d$, stability condition (45) in Sect. 3 is investigated. When there is just one or no point in the frequency-response curve corresponding to

$$b_{11}b_{22} - b_{12}b_{21} = 0, \tag{52}$$

the jump will be avoided. So the boundary between jump avoidance and jump occurrence regions can be determined by combining Eq. (52) and frequency-response Eq. (26).

It can be obtained that there is a minimum value of ξ_2 corresponding to every set of ρ and d for a certain primary isolator to avoid the jump. In Fig. 6, it can be seen that when the free travel d is equal or less 3.5, condition (51) is satisfied for $|\mu| = 0.01$ and $\xi_2 = 0.03$. The minimum values of ξ_2 for different sets of ρ and d construct a surface plot as shown in Fig. 7. This surface plot defines the boundary between jump avoidance and jump occurrence regions. The jump will not occur when the parameter values of the end-stop are above or on the surfaces.

From the two-dimensional plots in Fig. 8, it can be seen further that $\xi_{2_\min}$ is more sensitive to the stiffness ratio ρ as the free travel d is increased for both the weakly and strongly hardening primary isolators. Nevertheless, for $\rho \leq 1$ and $d \leq 2$, the values of $\xi_{2_\min}$ are smaller and less sensitive. The results suggest that as long as the parameters ρ and d are in appropriate ranges, not too much damping of end-stops will be needed to avoid the jump in a hardening primary system although the positive stiffness and a smaller free travel of the buffer also bring a hard nonlinearity.

In Fig. 9a, b, it can be seen that less damping is needed to avoid a jump when $\rho \leq 1$ for a weakly softening primary isolator, where also $\xi_{2_\min}$ is less sensitive to the free travel d. In Fig. 9c, d, when ρ is increased to 1.5 for a strongly softening primary isolator with $\mu = -0.1$, also the values of $\xi_{2_\min}$ are small. Furthermore, a bit more damping is needed to avoid a jump for $\rho = 0$ and $\rho = 0.5$ than that for $\rho = 1$ and $\rho = 1.5$ in a strongly softening primary system. Then, it can be inferred that $\rho = 1$ is a preferable choice to avoid a jump for a softening primary system. A little bigger value of ρ than 1 is also a good choice for a strongly softening primary system.

6 Absolute acceleration response

Besides relative displacement response, absolute acceleration response of the mass m also is an important index to evaluate the performance of the vehicle suspension. The absolute acceleration response $\ddot{x}_1$ of the

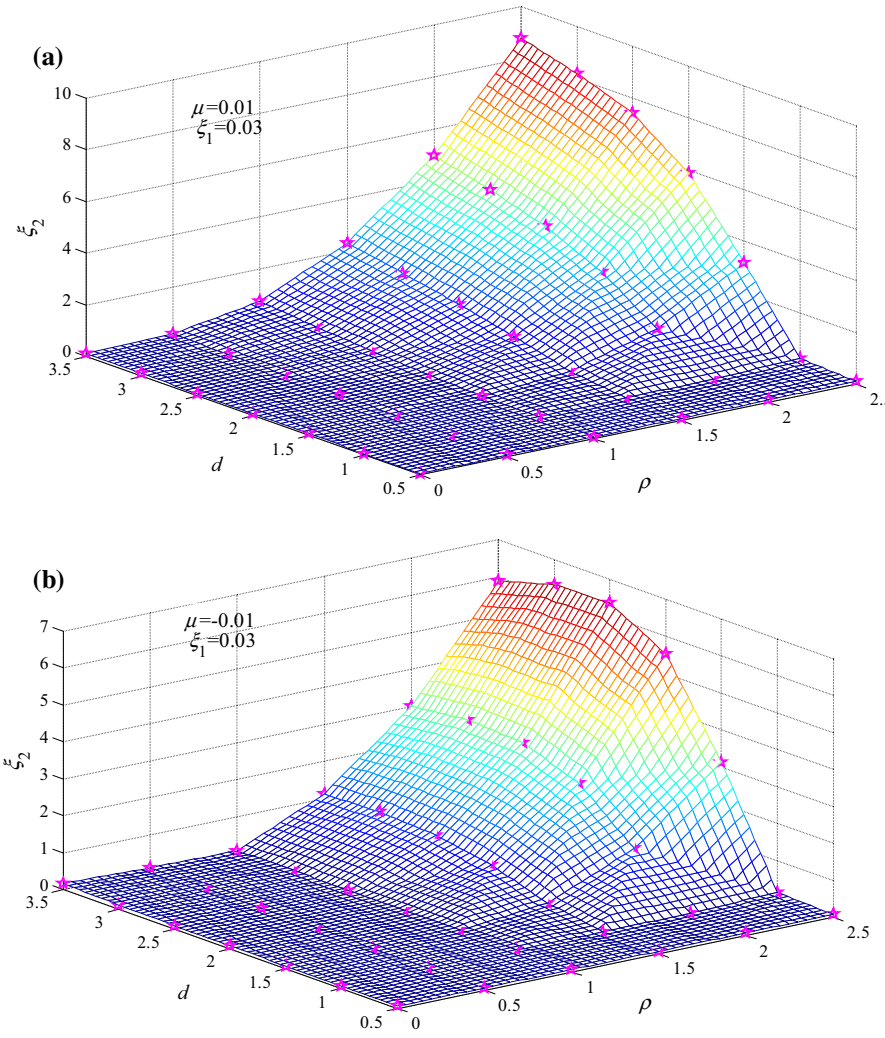


Fig. 7 Jump avoidance boundary surfaces when $|\mu| = 0.01$ and $\xi_1 = 0.03$: The pentagrams denote the points for surface interpolation

system after nondimensionalization is given by

$$\ddot{x}_1 = \ddot{y} + \ddot{x}_0 \tag{53}$$

where $x_1 = \frac{\hat{x}_1}{u_0}$ and $x_0 = \frac{\hat{x}_0}{u_0}$.

According to Eq. (11), the first-order approximation to the steady-state solution of Eq. (2) is

$$y \approx A\cos(\lambda\tau + \phi) \tag{54}$$

where A and ϕ are determined by Eqs. (20) and (21). The relative acceleration response in the steady state then can be written as

$$\ddot{y} \approx -A\lambda^2\cos(\lambda\tau + \phi) \tag{55}$$

Substituting Eq. (55) into Eq. (53) gives

$$\begin{aligned}\ddot{x}_1 &= -A\lambda^2\cos(\lambda\tau + \phi) - \lambda^2\cos\lambda\tau \\ &= (-A\lambda^2\cos\phi - \lambda^2)\cos\lambda\tau + A\lambda^2\sin\phi\sin\lambda\tau\end{aligned} \tag{56}$$

It can be combined with Eqs. (20) and (21) to give the amplitude of the absolute acceleration response as the function of A and λ:

$$\begin{aligned}X_{1_a} &= (A^2\lambda^4 + 2A\lambda^4\cos\phi + \lambda^4)^{1/2} \\ &= \left(A^2\lambda^4 + 2A\lambda^2\left(\rho^2(a_0 - a_2)A\right.\right. \\ &\quad \left.\left. -(\lambda^2 - 1)A + \frac{3}{4}\mu A^3\right) + \lambda^4\right)^{1/2}\end{aligned} \tag{57}$$

Effects of the design parameters of the end-stop, ρ, ξ_2 and d, on the absolute acceleration response are examined as shown in Figs. 10, 11 and 12, where the dotted lines represent values of the ampli-

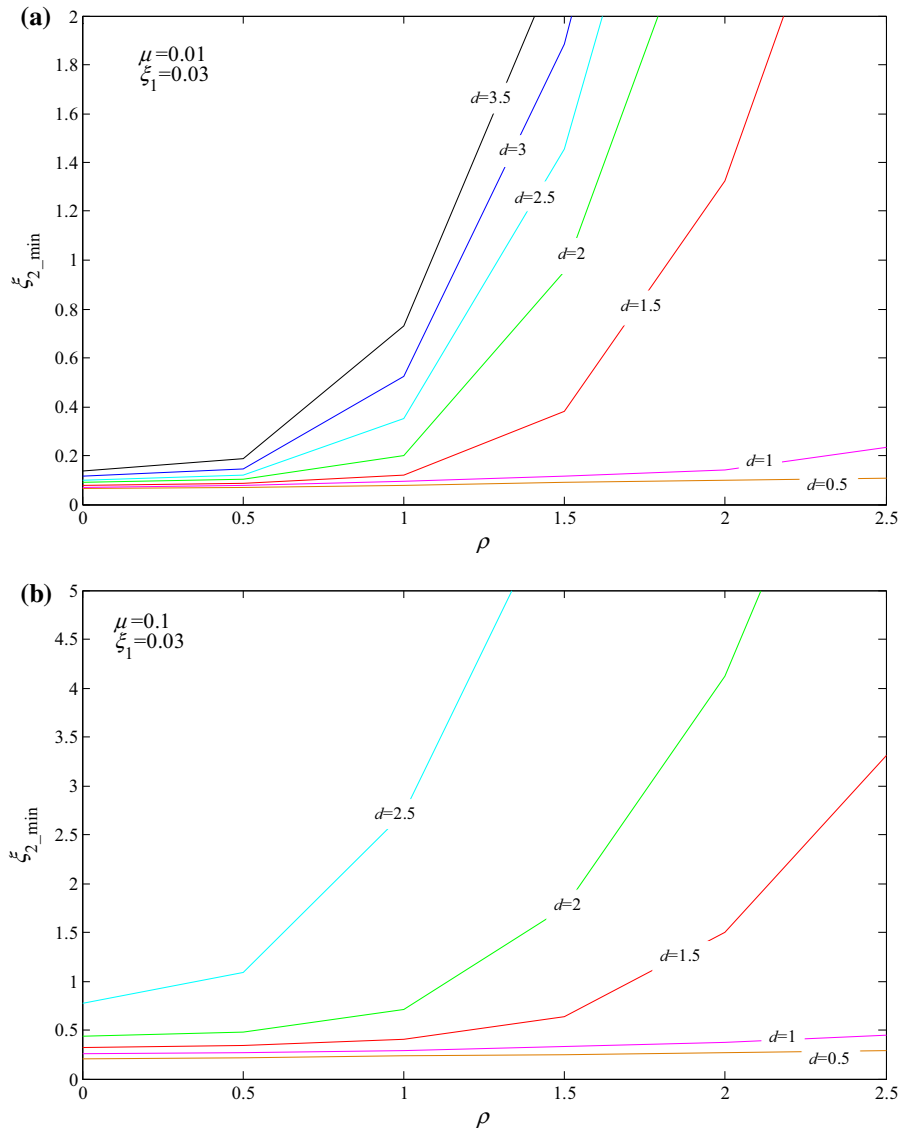


Fig. 8 Two-dimensional plots of ξ_{2_min} versus ρ for various values of d and for hardening primary isolators

tude X_{1_a} when $A = d$. From Figs. 10a, 11a and 12a, it can be seen that there is the similar effect to that on the relative displacement response. Also the results show that the viscoelastic end-stop can effectively attenuate the amplitude of the absolute acceleration response for a hardening primary isolator.

But on the other hand, as shown in Figs. 10b, 11b and 12b, the effect is quite different from that on the relative displacement response; the softening nonlinearity can be weaken, though. Comparing Fig. 10b with Fig. 4b, amplitude of the absolute acceleration response is more sensitive to the stiffness ratio ρ than that of the relative displacement response. Still, the amplitude of the absolute acceleration response will become lower as ξ_2 increases as shown in Fig. 11b. But more damping is needed for effective amplitude attenuation. Besides, in Fig. 12b, c, it is seen that the amplitudes of the absolute acceleration responses are increased and the response curves shift toward the right as d decreases for both the weakly and strongly softening primary isolators.

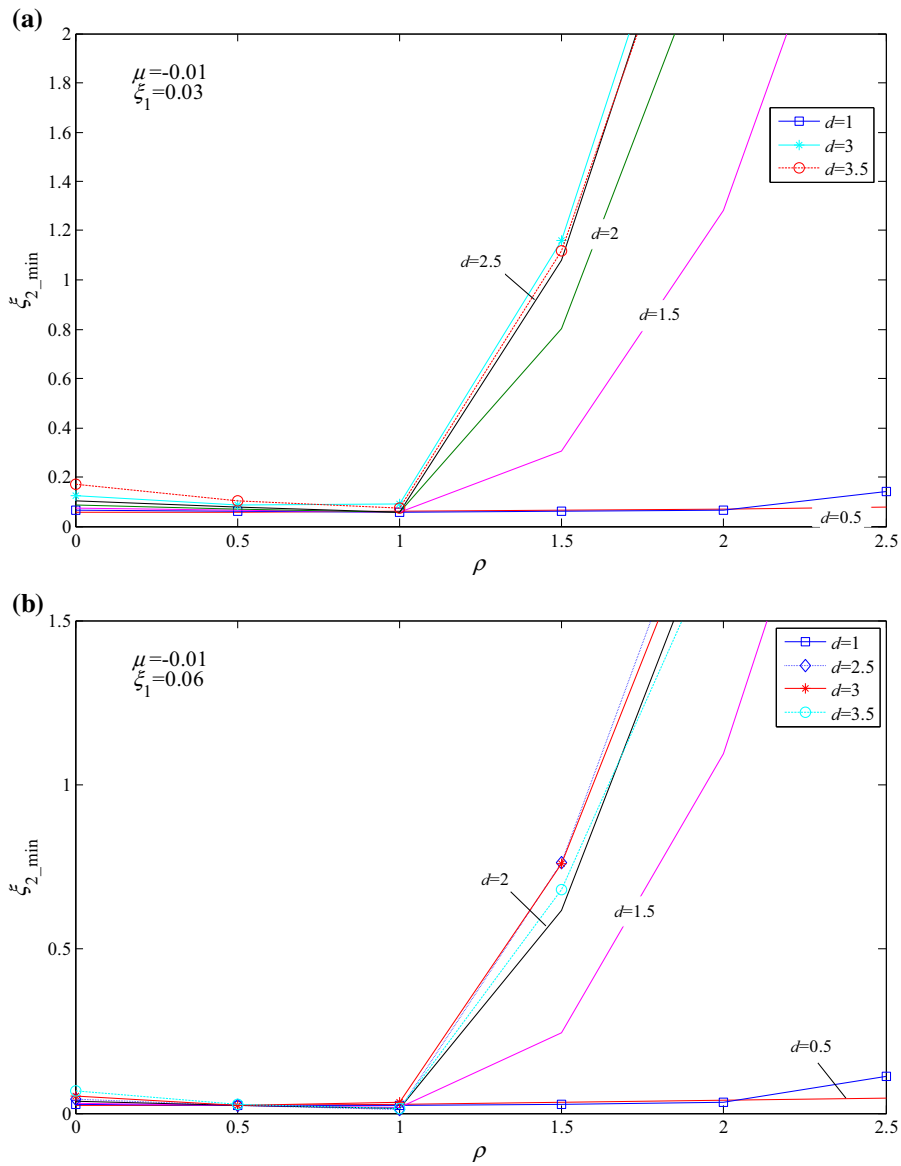
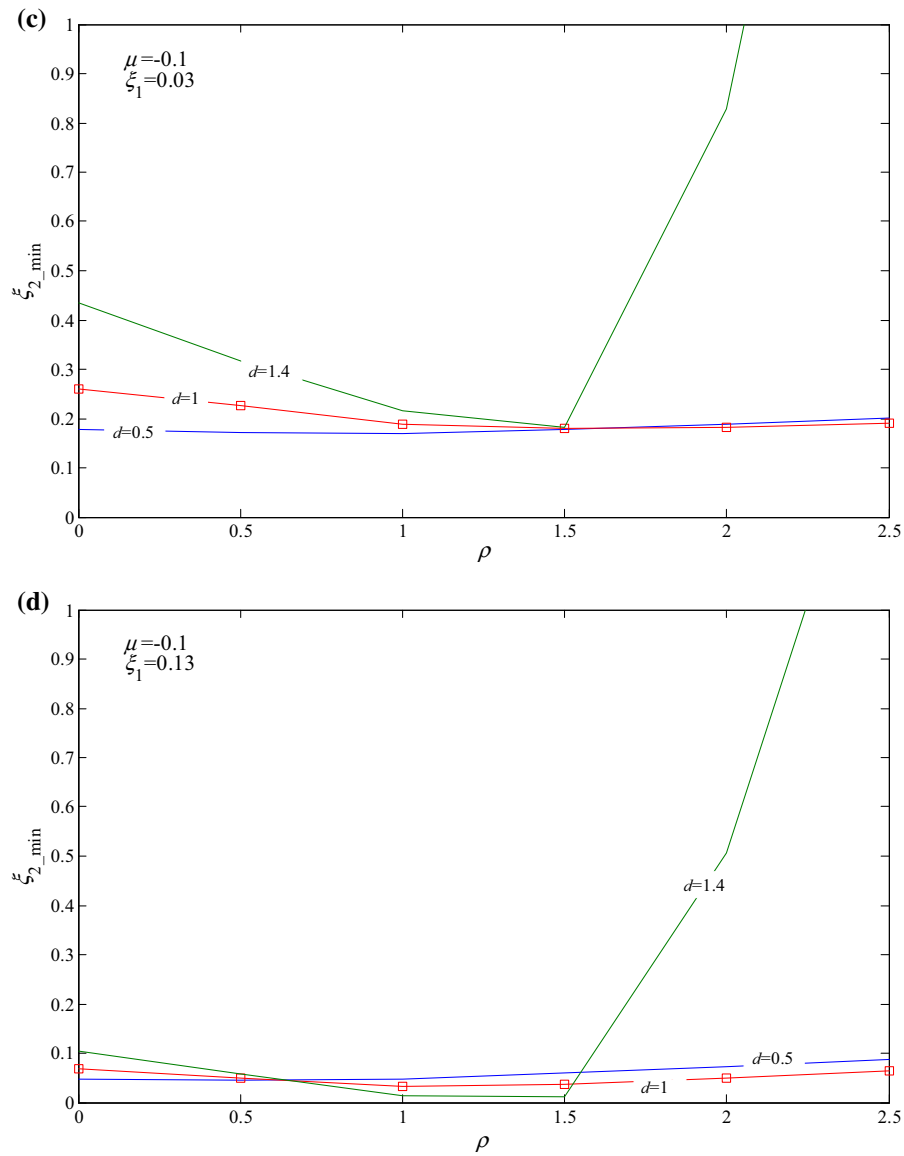


Fig. 9 Two-dimensional plots of ξ_{2_min} versus ρ for various values of d and for softening primary isolators

7 Conclusions

The present paper has studied the vibration isolation performance of a harmonically excited duffing-type suspension system with a pair of symmetric viscoelastic buffers under primary resonance conditions. A piecewise symmetry tri-nonlinear model is introduced to describe the dynamic behavior of the suspension system. The frequency response of the relative displacement obtained by the modified multiple-scale method completely agrees with the averaging method solution. Compared with the system without end-stops, the isolation performance at primary resonance becomes worse by using a pair of symmetric positive stiffness end-stops, while it is beneficial for vibration suppression by using damping end-stops. For the use of viscoelastic end-stops with appropriate positive parameters, the resonant response of relative displacement can be suppressed and the jump zone can be reduced effectively. The damping of end-

Fig. 9 continued



stops has benefit to the primary resonance mitigation, although a hardening nonlinearity is brought because of the stiffness and the free travel. It has been shown that the three design parameters, the stiffness ratio, the damping ratio and the free travel, of viscoelastic end-stops have interactive influence of each other on the isolation performance of the piecewise system.

The stability of the steady-state motion is determined by investigating the nature of the singular points, and jump avoidance conditions are subsequently investigated. There is a minimum value of ξ_2 corresponding to every set of ρ and d for a certain primary isolator to avoid the jump. $\rho = 1$ is a fairly good choice for jump avoidance for a softening primary system and also for a hardening primary system when d is in an appropriate range. The optimum parameters of the end-stop should be sought in the future because jump avoidance conditions are also dependent upon the nonlinearity and the damping of the primary isolator. Finally,

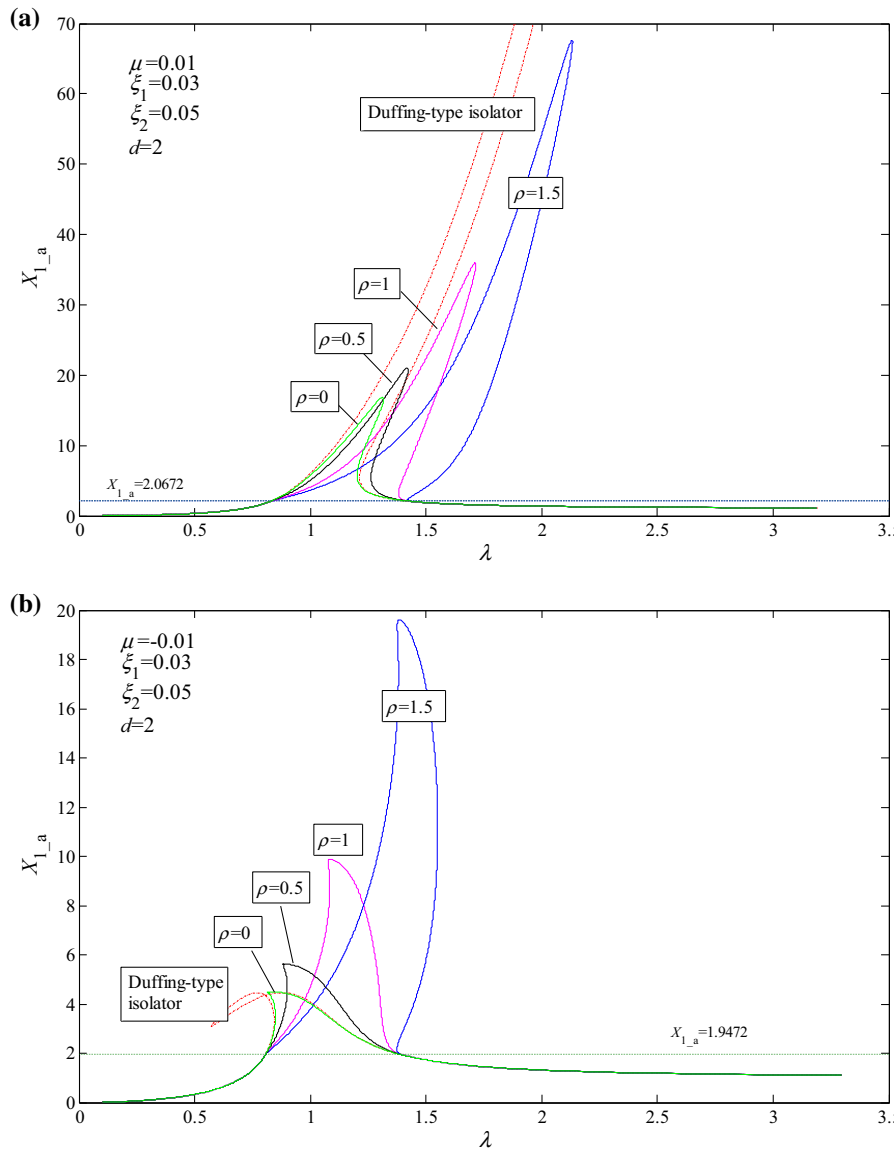


Fig. 10 Absolute acceleration response curves for various values of stiffness ratio ρ

effect of the end-stop design parameters on the absolute acceleration response is studied. It is demonstrated that for a hardening primary isolator, the viscoelastic end-stop can effectively attenuate the amplitude of the absolute acceleration response, which is similar to the response mitigation of relative displacement. But for a softening primary isolator, the end-stop should have more damping to attenuate the amplitude of the absolute acceleration response. Decrease of the free travel d results in acceleration response amplification for both the weakly and strongly softening primary isolators.

The main contribution of this study is the examination of the primary resonance response for the nonlinear suspension system. In further research, the authors will work on sub- and super-harmonic resonant solutions. And the study of energy consumption is also an important part of the future research.

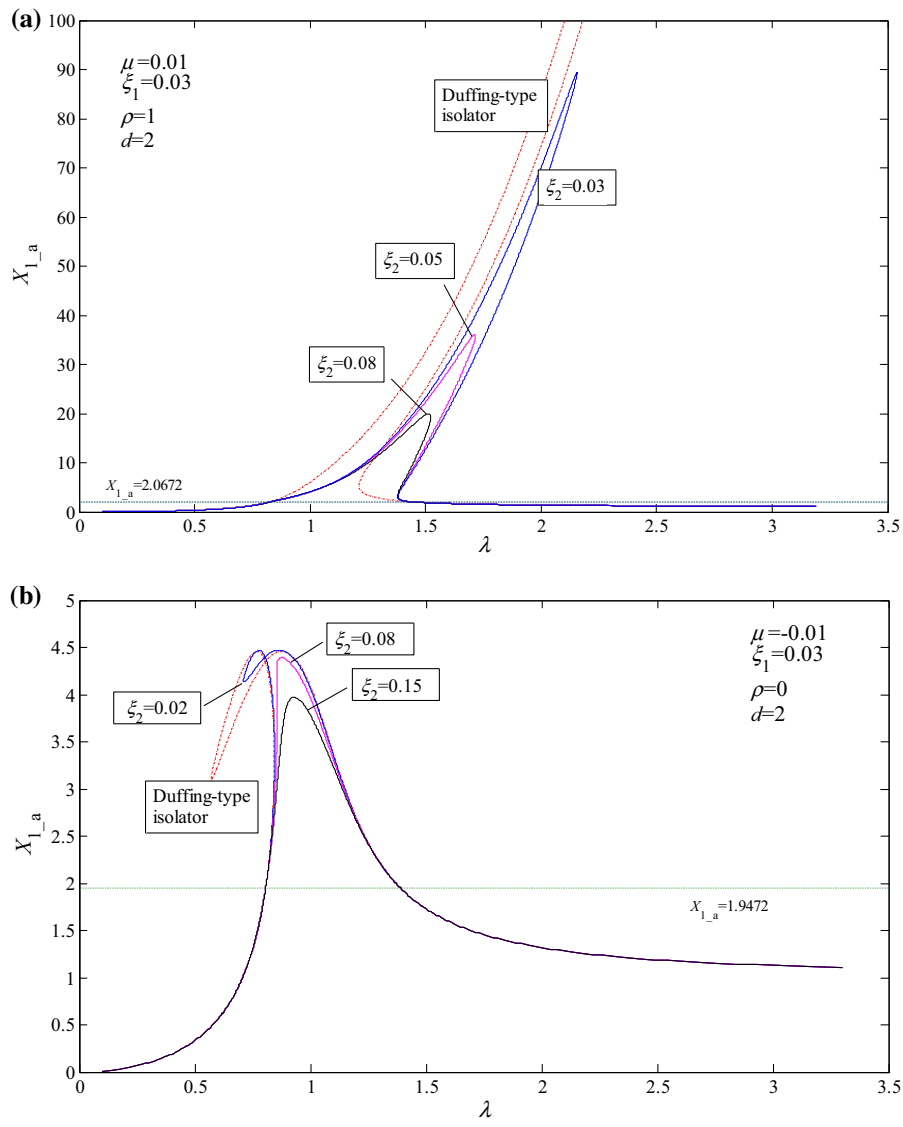


Fig. 11 Absolute acceleration response curves for various values of damping ξ_2

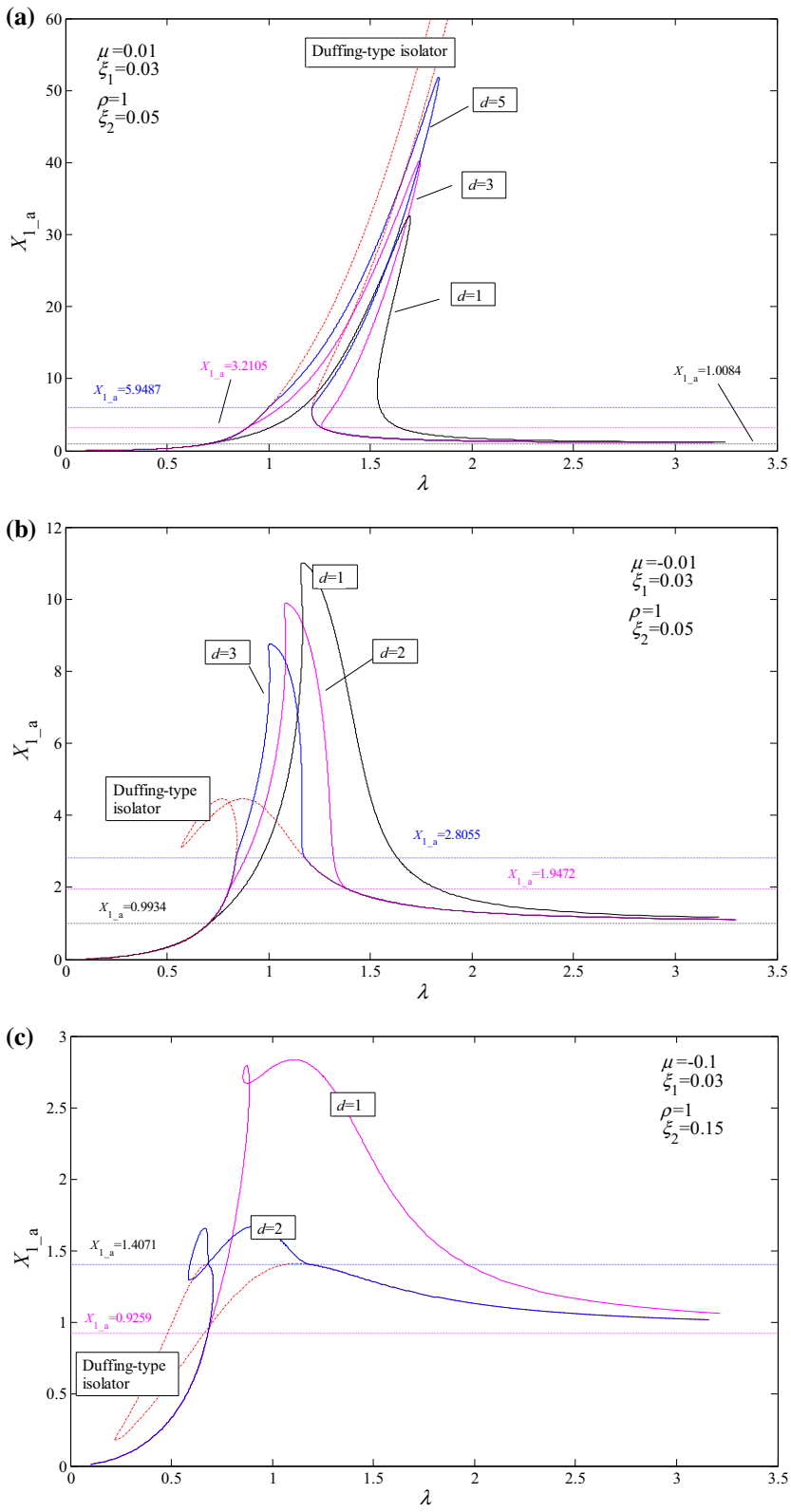


Fig. 12 Absolute acceleration response curves for various values of free travel *d*

Acknowledgements This work was supported by the Dr. Scientific Research Foundation of Taiyuan University of Science and Technology (Grant No. 20142035), the Natural Science Foundation Project of Shanxi Province China (Grant No. 201701D121069) and the National Natural Science Foundation of China (Grant Nos. 51775565, 51208500).

Compliance with ethical standards

Conflict of interests The authors declare that there is no conflict of interests regarding the publication of this article.

Appendix A

Using the averaging method

$$Y = \bar{A}(\tau)\cos(\lambda\tau + \bar{\gamma}(\tau)) \tag{A1}$$

$$\dot{Y} = -\bar{A}\lambda\sin(\lambda\tau + \bar{\gamma}) \tag{A2}$$

Then, the following equation is implied

$$\dot{\bar{A}}\cos(\lambda\tau + \bar{\gamma}) - \bar{A}\dot{\bar{\gamma}}\sin(\lambda\tau + \bar{\gamma}) = 0 \tag{A3}$$

And the acceleration is

$$\begin{aligned}\ddot{Y} = &-\dot{\bar{A}}\lambda\sin(\lambda\tau + \bar{\gamma}) - \bar{A}\lambda^2\cos(\lambda\tau + \bar{\gamma})\\ &-\bar{A}\dot{\bar{\gamma}}\lambda\cos(\lambda\tau + \bar{\gamma})\end{aligned} \tag{A4}$$

Considering $\varphi = \lambda\tau + \bar{\gamma}$ and defining $\varphi_0 = \begin{cases}\arccos\frac{d}{\bar{A}} \in \left(0, \frac{\pi}{2}\right) & \bar{A} > d\\ 0 & \bar{A} \le d\end{cases}$, substitute (A1), (A2) and (A4) into Eq. (2)

$$\begin{aligned}&-\dot{\bar{A}}\lambda\sin\varphi - \bar{A}\lambda(\lambda + \dot{\bar{\gamma}})\cos\varphi + \bar{A}\cos\varphi\\ &\quad + \mu\bar{A}^3\cos^3\varphi - 2\xi_1\bar{A}\lambda\sin\varphi + G_1\\ &\quad = \lambda^2\cos(\varphi - \bar{\gamma})\end{aligned} \tag{A5}$$

where

$$G_1 = \begin{cases}\rho^2(\bar{A}\cos\varphi - d) - 2\xi_2\bar{A}\lambda\sin\varphi & 0 < \varphi < \varphi_0 \quad \text{or} \quad 2\pi - \varphi_0 < \varphi < 2\pi\\ 0 & \varphi_0 \le \varphi \le \pi - \varphi_0 \quad \text{or} \quad \pi + \varphi_0 \le \varphi \le 2\pi - \varphi_0\\ \rho^2(\bar{A}\cos\varphi + d) - 2\xi_2\bar{A}\lambda\sin\varphi & \pi - \varphi_0 < \varphi < \pi + \varphi_0\end{cases}$$

Because only $\varphi_0 \le \varphi \le \pi - \varphi_0$ or $\pi + \varphi_0 \le \varphi \le 2\pi - \varphi_0$ can be true when $\varphi_0 = 0$, G_1 is true under both conditions of $A > d$ and $A \le d$.

Solving Eqs. (A3) and (A5) for $\dot{\bar{A}}$ and $\dot{\bar{\gamma}}$, we have

$$\begin{aligned}\lambda\dot{\bar{A}} = &-\bar{A}(\lambda^2 - 1)\cos\varphi\sin\varphi + \mu\bar{A}^3\cos^3\varphi\sin\varphi\\ &-2\xi_1\bar{A}\lambda\sin^2\varphi + G_1\sin\varphi\\ &-\lambda^2\cos(\varphi - \bar{\gamma})\sin\varphi\end{aligned} \tag{A6}$$

$$\begin{aligned}\lambda\bar{A}\dot{\bar{\gamma}} = &-\bar{A}(\lambda^2 - 1)\cos^2\varphi + \mu\bar{A}^3\cos^4\varphi\\ &-2\xi_1\bar{A}\lambda\sin\varphi\cos\varphi + G_1\cos\varphi\\ &-\lambda^2\cos(\varphi - \bar{\gamma})\cos\varphi\end{aligned} \tag{A7}$$

Averaging them over the period $2\pi/\lambda$, we have

$$\begin{aligned}\lambda\dot{\bar{A}} = &-\xi_1\lambda\bar{A} - \frac{1}{\pi}\xi_2\lambda\bar{A}(2\varphi_0 - \sin 2\varphi_0)\\ &-\frac{1}{2}\lambda^2\sin\bar{\gamma}\end{aligned} \tag{A8}$$

$$\begin{aligned}\lambda\bar{A}\dot{\bar{\gamma}} = &-\frac{1}{2}\bar{A}(\lambda^2 - 1) + \frac{3}{8}\mu\bar{A}^3\\ &+\frac{1}{2\pi}(2\rho^2\bar{A}\varphi_0 - 4d\rho^2\sin\varphi_0 + \rho^2\bar{A}\sin 2\varphi_0)\\ &-\frac{1}{2}\lambda^2\cos\bar{\gamma}\end{aligned} \tag{A9}$$

At the steady-state condition, the derivatives $\dot{A}$ and $\dot{\bar{\gamma}}$ can be considered to be zero. Then,

$$\lambda^2\sin\bar{\gamma} = -2\xi_1\lambda\bar{A} - \frac{2}{\pi}\xi_2\lambda\bar{A}(2\varphi_0 - \sin 2\varphi_0) \tag{A10}$$

$$\begin{aligned}\lambda^2\cos\bar{\gamma} = &-\bar{A}(\lambda^2 - 1) + \frac{3}{4}\mu\bar{A}^3\\ &+\frac{1}{\pi}\Big(2\rho^2\bar{A}\varphi_0 - 4d\rho^2\sin\varphi_0\\ &+\rho^2\bar{A}\sin 2\varphi_0\Big)\end{aligned} \tag{A11}$$

Therefore,

$$\begin{aligned}&\left[-\bar{A}(\lambda^2 - 1) + \frac{3}{4}\mu\bar{A}^3\right.\\ &\left.+\frac{\rho^2}{\pi}(2\bar{A}\varphi_0 - 4d\sin\varphi_0 + \bar{A}\sin 2\varphi_0)\right]^2\\ &+\bar{A}^2\lambda^2\left[2\xi_1 + \frac{2}{\pi}\xi_2(2\varphi_0 - \sin 2\varphi_0)\right]^2 = \lambda^4\end{aligned} \tag{A12}$$

Appendix B

$$R_1'(A) = \frac{2a_2\rho^2}{A} \tag{B1}$$

$$R_2'(A) = \frac{4a_2\xi_2}{A} \tag{B2}$$

References

1. Wu, X., Griffin, M.J.: The influence of end-stop buffer characteristics on the severity of suspension seat end-stop impacts. J. Sound Vib. **215**(4), 989–996 (1998)
2. Lemerle, P., Boulanger, P., Poirot, R.: A simplified method to design suspended cabs for counterbalance trucks. J. Sound Vib. **253**(1), 283–293 (2002)
3. Rakheja, S., Boileau, P.-É., Wang, Z., et al.: Performance analysis of suspension seats under high magnitude vibration excitations: part I: model development and validation. J. Low Freq. Noise Vib. Act. Control **22**(4), 225–252 (2003)
4. Gunston, T.P., Rebelle, J., Griffin, M.J.: A comparison of two methods of simulating seat suspension dynamic performance. J. Sound Vib. **278**(1), 117–134 (2004)
5. Rebelle, J.: Methodology to improve the performance of the end-stop buffers of suspension seats. Veh. Syst. Dyn. **42**(4), 211–233 (2004)
6. Zhou, C., Sun, B., Chen, N., et al.: Ride comfort simulation and experimental research of nonlinear rubber suspension system. J. Southeast Univ. (Nat. Sci. Ed.) **37**(1), 30–34 (2007). (in Chinese with English abstract)
7. Milburn, R.J., Bakken, M., Virgilio, S., et al.: Cab suspension system for an off-road vehicle. US Patent No. 8,807,633 B2 (2014)
8. Zhong, S., Chen, Y.: Bifurcation of piecewise-linear nonlinear vibration system of vehicle suspension. Appl. Math. Mech. (Engl. Ed.) **30**(6), 677–684 (2009)
9. Le, V.Q., Zhang, J., Liu, X., et al.: Nonlinear dynamic analysis of interaction between vehicle and road surfaces for 5-axle heavy truck. J. Southeast Univ. (Engl. Ed.) **27**(4), 405–409 (2011)
10. Ward, C.H.: The application of a new cab mounting to address cab shake on the 2003 Chevrolet Kodiak and GMC Topkick. In: SAE Technical Paper Series 2002-01-3102
11. Sun, X., Zhang, J.: Performance of earth-moving machinery cab with hydraulic mounts in low frequency. J. Vib. Control **20**(5), 724–735 (2014)
12. Tuncel, O., Sendur, P., Özkan, M., et al.: Technical note: ride comfort optimization of Ford cargo truck cabin. Int. J. Veh. Des. **52**(1), 222–236 (2010)
13. Naraynan, S., Sekar, P.: Periodic and chaotic responses of an SDF system with piecewise linear stiffness subjected to combined harmonic and flow induced excitations. J. Sound Vib. **184**(2), 281–298 (1995)
14. Ing, J., Pavlovskaia, E., Wiercigroch, M.: Dynamics of a nearly symmetrical piecewise linear oscillator close to grazing incidence: modelling and experimental verification. Nonlinear Dyn. **46**, 225–238 (2006)
15. Ing, J., Pavlovskaia, E., Wiercigroch, M., Banerjee, S.: Experimental study of impact oscillator with one-sided elastic constraint. Philos. Trans. R. Soc. A **366**, 679–704 (2008)
16. Liu, Y., Pavlovskaia, E., Wiercigroch, M.: Experimental verification of the vibro-impact capsule model. Nonlinear Dyn. **83**, 1029–1041 (2016)
17. Wiercigroch, M., Sin, V.W.T.: Experimental study of a symmetrical piecewise base-excited oscillator. ASME J. Appl. Mech. **65**, 657–663 (1998)
18. Narimani, A., Golnaraghi, M.F., Jazar, R.N.: Optimizing piecewise linear isolator for steady state vibration. In: Proceedings of IMECE'03 2003 ASME International Mechanical Engineering Congress, Washington, D.C., Nov. 15–21 (2003)
19. Narimani, A., Golnaraghi, M.F., Jazar, G.N.: Frequency response of a piecewise linear vibration isolator. J. Vib. Control **10**, 1775–1794 (2004)
20. Deshpande, S., Mehta, S., Jazar, G.N.: Optimization of secondary suspension of piecewise linear vibration isolation systems. Int. J. Mech. Sci. **48**(4), 341–377 (2006)
21. Jazar, G.N., Mahinfalah, M., Deshpande, S.: Design of a piecewise linear vibration isolator for jump avoidance. Proc. Inst. Mech. Eng. Part K **221**(3), 441–450 (2007)
22. Wallentowitz, H.: Automotive Engineering II: Vertical and Lateral Dynamics of Vehicles. China Machine Press, Beijing (2009)
23. Mallik, A.K., Kher, V., Puri, M., Hatwal, H.: On the modeling of non-linear elastomeric vibration isolators. J. Sound Vib. **219**(2), 239–253 (1999)
24. Shaska, K., Ibrahim, R.A., Gibson, R.F.: Influence of excitation amplitude on the characteristics of nonlinear butyl rubber isolators. Nonlinear Dyn. **47**, 83–104 (2007)
25. Natsiavas, S., Tratskas, P.: On vibration isolation of mechanical systems with non-linear foundations. J. Sound Vib. **194**(2), 173–185 (1996)
26. Stahl, P., Jazar, G.N.: Frequency response analysis of piecewise nonlinear vibration isolator. In: Proceedings of IDETC/CIE 2005, ASME International Design Engineering Technical Conferences and Computers and Information in Engineering Conference, Long Beach, CA, USA, Sept. 24–28 (2005)
27. Stahl, P., Jazar, G.N.: Stability analysis of a piecewise nonlinear vibration isolator. In: Proceedings of IMECE2005, ASME International Mechanical Engineering Congress and Exposition, Orlando, FL, USA, Nov. 5–11 (2005)
28. Hao, Z., Cao, Q., Wiercigroch, M.: Two-sided damping constraint control strategy for high-performance vibration isolation and end-stop impact protection. Nonlinear Dyn. **86**(4), 1–16 (2016)
29. Andreaus, U., De Angelis, M.: Nonlinear dynamic response of a base-excited SDOF oscillator with double-side unilateral constraints. Nonlinear Dyn. **84**(3), 1447–1467 (2016)
30. Yan, Y., Liu, Y., Liao, M.: A comparative study of the vibro-impact capsule systems with one-sided and two-sided constraints. Nonlinear Dyn. **89**, 1063–1087 (2017)
31. Liu, Y., Páez, Chávez J.: Controlling multistability in a vibro-impact capsule system. Nonlinear Dyn. **88**, 1289–1304 (2017)
32. Gao, X., Chen, Q.: Nonlinear frequency response analysis and dynamics design of a solid and liquid mixture nonlinear vibration isolator. J. Vib. Control **20**(15), 2389–2400 (2013)
33. Gao, X., Chen, Q.: Nonlinear analysis, design and vibration isolation for a bilinear system with time-delayed cubic velocity feedback. J. Sound Vib. **333**(6), 1562–1576 (2014)
34. Cheng, C., Li, S., Wang, Y., et al.: On the analysis of a high-static-low-dynamic stiffness vibration isolator with time-delayed cubic displacement feedback. J. Sound Vib. **378**, 76–91 (2016)
35. Sun, B., Zhou, C., Zhang, X., et al.: Nonlinear dynamic characteristics of rubber suspension of construction vehicle. J. Southeast Univ. (Nat. Sci. Ed.) **37**(6), 974–979 (2007). (in Chinese with English abstract)

36. Nayfeh, A.H., Mook, D.T.: Nonlinear Oscillations. Wiley-VCH Verlag GmbH & Co. KGaA, Weinheim (2004)
37. Kandil, A., Eissa, M.: Improvement of positive position feedback controller for suppressing compressor blade oscillations. Nonlinear Dyn. **90**(3), 1727–1753 (2017)
38. Li, L., Zhang, Q., Wang, W., et al.: Nonlinear coupled vibration of electrostatically actuated clamped-clamped microbeams under higher-order modes excitation. Nonlinear Dyn. **90**(3), 1593–1606 (2017)
39. Liu, F., Xiang, C., Liu, H., et al.: Nonlinear vibration of permanent magnet synchronous motors in electric vehicles influenced by static angle eccentricity. Nonlinear Dyn. **90**(3), 1851–1872 (2017)
40. Babitsky, V.I., Veprik, A.M.: Universal bumpered vibration isolator for severe environment. J. Sound Vib. **218**(2), 269–292 (1998)
41. Zhang, R., Li, K., Yu, F., et al.: Novel electronic braking system design for EVS based on constrained nonlinear hierarchical control. Int. J. Automot. Technol. **18**(4), 707–718 (2017)
42. Zhang, R.H., Ma, Y.B., You, F., Peng, T., He, Z.C., Li, K.N.: Exploring to direct the reaction pathway for hydrogenation of levulinic acid into gvalerolactone for future clean-energy vehicles over a magnetic Cu–Ni catalyst. Int. J. Hydrog. Energy **42**(40), 25185–25194 (2017)
43. Brennan, M.J., Kovacic, I., Carrella, A., Waters, T.P.: On the jump-up and jump-down frequencies of the duffing oscillator. J. Sound Vib. **318**, 1250–1261 (2008)
44. Zhang, R.H., He, Z.C., Wang, H.W., You, F., Li, K.N.: Study on self-tuning tyre friction control for developing main-servo loop integrated chassis control system. IEEE Access **5**, 6649–6660 (2017)
45. You, F., Zhang, R., Guo, L., et al.: Trajectory planning and tracking control for autonomous lane change maneuver based on the cooperative vehicle infrastructure system. Exp. Syst. Appl. **42**(14), 5932–5946 (2015)
46. Song, H., Zheng, P., Ge, H.: TDGL and mKdV equations for an extended car-following model. Nonlinear Dyn. **90**(4), 2253–2262 (2017)
47. Zhang, R., Li, K., He, Z., et al.: Advanced emergency braking control based on a nonlinear model predictive algorithm for intelligent vehicles. Appl. Sci. **7**(5), 504 (2017)